Electronic Supplementary Material (ESI) for Dalton Transactions.
This journal is © The Royal Society of Chemistry 2022

Supporting Information

One-pot Production of Sea Urchin-Like Alloy Electrocatalyst for Oxygen Electro-Reduction Reaction

Hau Quoc Pham,[1,2] and Tai Thien Huynh[3,]*

[1]Future Materials & Devices Lab., Institute of Fundamental and Applied Sciences, Duy Tan University, Ho Chi Minh City, 700000, Viet Nam

[2]The Faculty of Environmental and Chemical Engineering, Duy Tan University, Da Nang, 550000, Viet Nam

[3]Ho Chi Minh City University of Natural Resources and Environment (HCMUNRE), Ho Chi Minh City, 700000, Viet Nam

*Corresponding author. E-mail: httai@hcmunre.edu.vn

EXPERIMENTAL DETAILS

Chemical reagents

All reagents were commercially purchased and used without further purification. Hexachloroplatinic acid ($H_2PtCl_6.xH_2O$; ~38% Pt), nickel(II) chloride hexahydrate ($NiCl_2.6H_2O$; 99.9% trace metal basis), and Nafion 117 solution (5 wt%) were purchased from Sigma-Aldrich, USA. Polyvinylpyrrolidone (PVP, MW = 40 000) and L-ascorbic acid (≥ 99.7%) were obtained from HiMedia Lab., India, and Beijing Chemical Reagent, China.

Material Characterizations

X-ray diffraction (XRD) pattern of as-made catalyst was collected on D2 PHASER (Bruker, Germany) with Cu K_α radiation source (λ = 1.5418 Å) in degree range of 20^o to 80^o at a step size of 0.02^o. The morphology and particle size of the as-obtained nanocatalyst were characterized through transmission electron microscopy (TEM) and HR-TEM images on a JOEL-JEM 2100F device at 200 kV. Before the test, a specimen was distributed in ethanol solution to form a homogeneous suspension, followed by casting on carbon film-coated copper microgrids. Also, elemental composition and distribution were recorded by scanning electron microscopy (SEM) with energy dispersive X-ray analysis (EDX) on JOEL-JSM 6500F device at 10 kV. X-ray photoelectron spectroscopy (XPS) was carried out on PHI 5000 VersaProbe (Ulvac-PHI) equipped with a monochromator Al K_α ($h\upsilon$ = 1486.6 eV) X-ray source at a 10 mV current and 15 kV anode voltage.

Electrochemical Properties

Electrochemical measurements were conducted on an Autolab potentiostat/galvanostat (PGSTAT302N) workstation (Metrohm Co., Ltd. Switzerland) connected with a three-electrode cell, including a working electrode (glassy carbon (GCE), 5 mm), a counter electrode (platinum wire), and reference electrode (Ag/AgCl/(sat.KCl). For catalyst ink preparation, 1.7 mg of as-made catalyst was dispersed in a mixture of 20 μL of Nafion and

180 μL of ethanol absolute, followed by the ultrasonication of 30 min to form a homogeneous ink. Before coasting the as-prepared catalyst ink, the surface of the working electrode was polished by 0.5 μm Al_2O_3 and washed by absolute ethanol and purged water, and then 2.5 μL of catalyst ink was drop-cast onto the GCE surface and dried naturally. To start with, a cyclic voltammetry test was performed in an N_2-saturated 0.5 M H_2SO_4 electrolyte solution with 100 cycles at 50 mV s^{-1} to get an active working electrode. The electrochemical surface area (ECSA) of the as-made catalyst was calculated from the hydrogen adsorption/desorption region in cyclic voltammetry (CV) in N_2-saturated 0.5 M H_2SO_4 aqueous electrolyte at 25 mV s^{-1} scan rate. To investigate the ORR performance, linear sweep voltammetry (LSV) test was carried out using a rotating disk electrode (Autolab RDE) at 1600 rpm in an O_2-saturated 0.5 M H_2SO_4 electrolyte solution at a scan rate of 10 mV s^{-1}. Electrochemical impedance spectroscopy (EIS) was recorded in a frequency range of 0.1 - 10^5 Hz at 0.9 V_{RHE} in an O_2-saturated 0.5 M H_2SO_4 electrolyte solution. In terms of electrocatalytic stability, an accelerated durability test (ADT) with 5000-cycling was conducted in N_2- and O_2-saturated 0.5 M H_2SO_4 electrolyte solution. For comparison, 20 wt% Pt NPs/C (E-TEK) catalyst was used as a benchmark catalyst. All reported potentials were converted from Ag/AgCl to reversible hydrogen electrode (RHE) scale by Eqs. (1)-(3):[1]

$$E_{RHE} = E_{Mea} + 0.059*pH + E^0_{Ag/AgCl} \quad (1)$$

$$E_{RHE} = E_{Mea} + 0.059*0 + 0.197 \quad (2)$$

$$E_{RHE} = E_{Mea} + 0.197 \quad (3)$$

where E_{RHE} is a potential versus RHE, E_{Mea} is a measured potential, $E^0_{Ag/AgCl}$ is a standard electrode potential of Ag/AgCl/(sat.KCl), and pH of 0.5 M H_2SO_4 is close to 0.

Calculation of lattice parameters of as-made NiPt NUCs/C catalyst

The interplanar spacing ($d_{(hkl)}$) was calculated by Bragg's law (Eq. (4))[2, 3]:

$$d_{(hkl)} = \frac{\lambda}{2\sin\theta} \quad (4)$$

where: $d_{(hkl)}$ is lattice space (Å); λ is the wavelength of the incident X-ray (λ = 15406 Å); θ is the Bragg angle.

The coherent length ($D_{(hkl)}$) was estimated by Debye-Scherrer's formula (Eq.(5))[2-4]:

$$D_{(hkl)} = \frac{k\lambda}{\beta\cos\theta} \quad (5)$$

where: $D_{(hkl)}$ is average crystallite size (nm), k is Scherrer constant (0.94), λ is the wavelength of the incident X-ray (λ = 15406 Å), β is the line broadening at half the maximum intensity (FWHM), and θ is the Bragg angle.

Calculation of electrochemical surface area

Based on hydrogen adsorption/desorption regions in CV curves in N_2-purged 0.5 M H_2SO_4 electrolyte solution, the electrochemical surface area (ECSA) of as-made NiPt NUCs/C and commercial Pt NPs/C (E-TEK) catalysts was calculated by Eq. (6):[5-7]

$$ECSA = \frac{Q_H}{0.21*[Metal]} \quad (6)$$

where Q_H (mC cm^{-2}) represents the coulombic charge for hydrogen adsorption; 0.21 (mC cm^{-2}) is the charge required to oxidize an H_2 monolayer, and [Metal] is the loaded catalyst metal onto the working surface electrode (0.13 mg cm^{-2}). Q_H can be estimated by Eqs. (7):[8, 9]

$$Q_H = \frac{1}{\nu A}\int I_{(V)}dV \quad (7)$$

where I (A) represents the peak current; V (V) is the peak potential; ν (mV s^{-1}) denotes the scanning rate, which is 25 mV s^{-1} in this experiment; and A (cm^{-2}) is the GCE's geometric area, which is 0.1964 cm^{-2}.

Calculation of ORR kinetics of catalyst

Based on the rotating disk electrodes (RDE) test, the kinetic current density and number of

transferred electrons during the oxygen electro-reduction process were calculated by Koutecky-Levich (K-L) equation as follows:[10-15]

$$\frac{1}{j} = \frac{1}{j_L} + \frac{1}{j_K} = \frac{1}{B\omega^{1/2}} + \frac{1}{j_K} \quad (8)$$

$$B = 0.201nFC_0D^{2/3}\nu^{-1/6} \quad (9)$$

where j (mA cm^{-2}) is a measured current density, j_L (mA cm^{-2}) and j_K (mA cm^{-2}) are diffusion-limited current density and kinetic current density, respectively. B (C cm^{-2} s$^{-1/2}$) is the Levich constant, which was calculated from slope values of $1/j$ and $1/\omega^{1/2}$; n is the transferred electron number during ORR; F (96485 C mol^{-1}) is the Faraday constant; C_0 is the bulk concentration of O_2 (1.17x10^{-6} mol cm^{-3} in 0.5 M H_2SO_4).[16, 17] D is the diffusion coefficient of O_2 (1.4x10^{-5} cm^2 s^{-1} in 0.5 M H_2SO_4)[16, 17]; ν is the kinematic viscosity of electrolyte (0.01 cm^2 s^{-1} for 0.5 M H_2SO_4);[16, 17] and ω (rad s$^{-1/2}$) is electrode angular velocity. Then, the kinetic current density was calculated following Eq. (10):

$$j_K = \frac{j * j_L}{j_L - j} \quad (10)$$

The mass activity and specific activity were calculated by following Eq.(11), (12):

$$Mass\ activity = \frac{j_K}{[Metal]} \quad (11)$$

$$Specific\ activity = \frac{Mass\ activity}{ECSA} \quad (12)$$

Results and Discussion

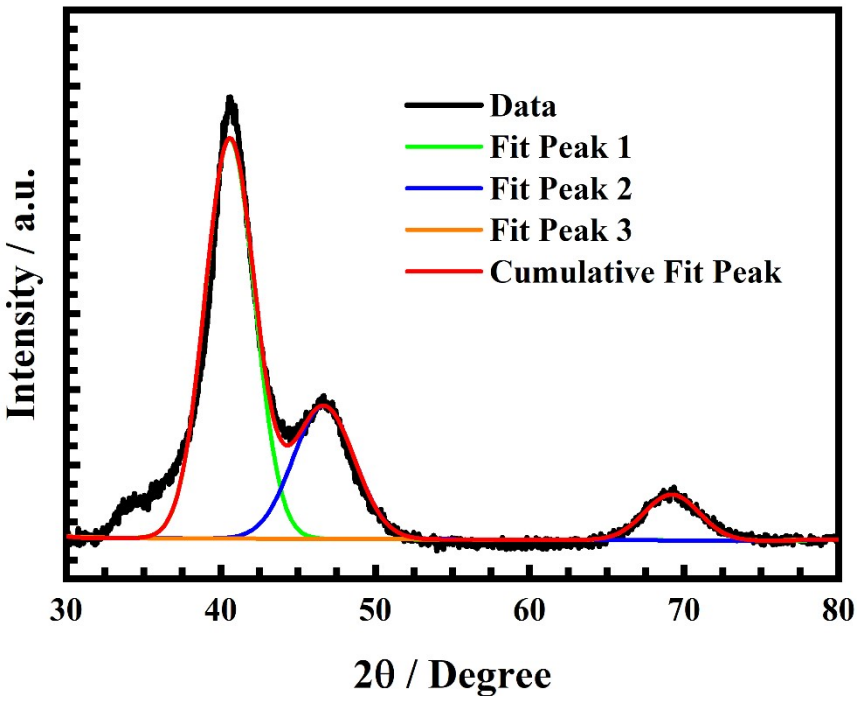

Figure S1. Fitted-XRD pattern of as-made NiPt NUCs/C catalyst.

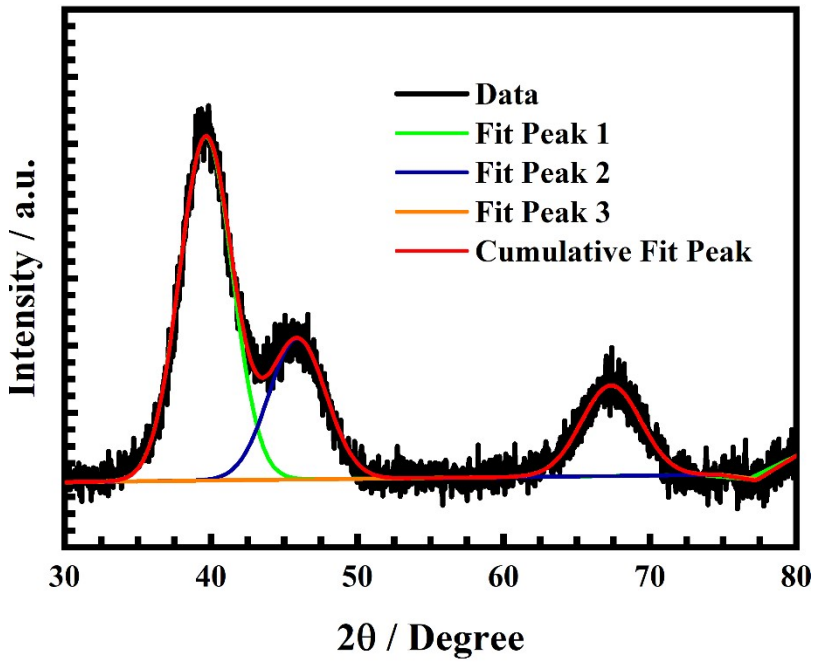

Figure S2. Fitted-XRD pattern of commercial Pt NPs/C catalyst.

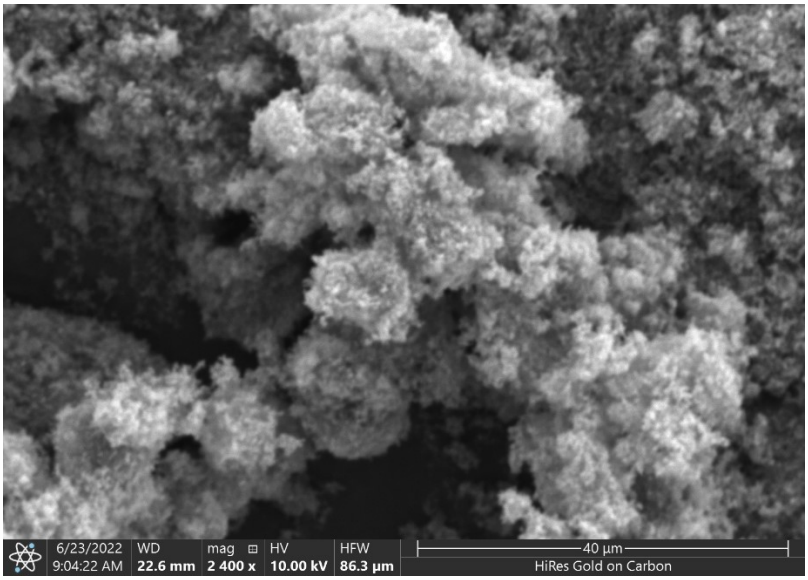

Figure S3. SEM image of the as-made NiPt NUCs/C catalyst.

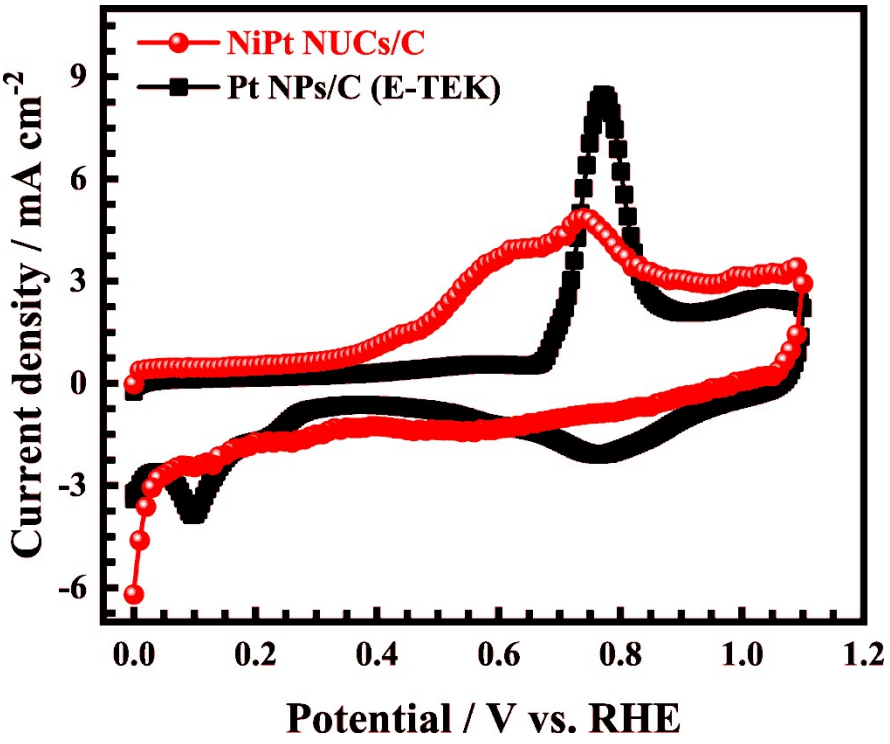

Figure S4. CO-stripping curves of as-made NiPt NUCs/C and Pt NPs/C (E-TEK) catalysts in 0.5 M H_2SO_4 electrolyte solution at a scan rate of 50 mV s^{-1}.

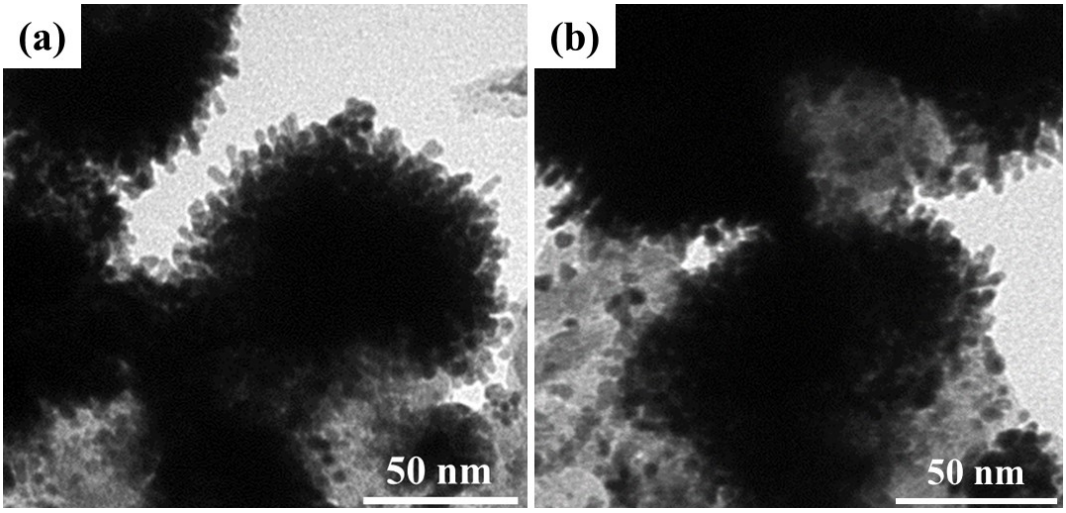

Figure S5. TEM images of the as-made NiPt NUCs/C catalyst (a) before and (b) after ADT.

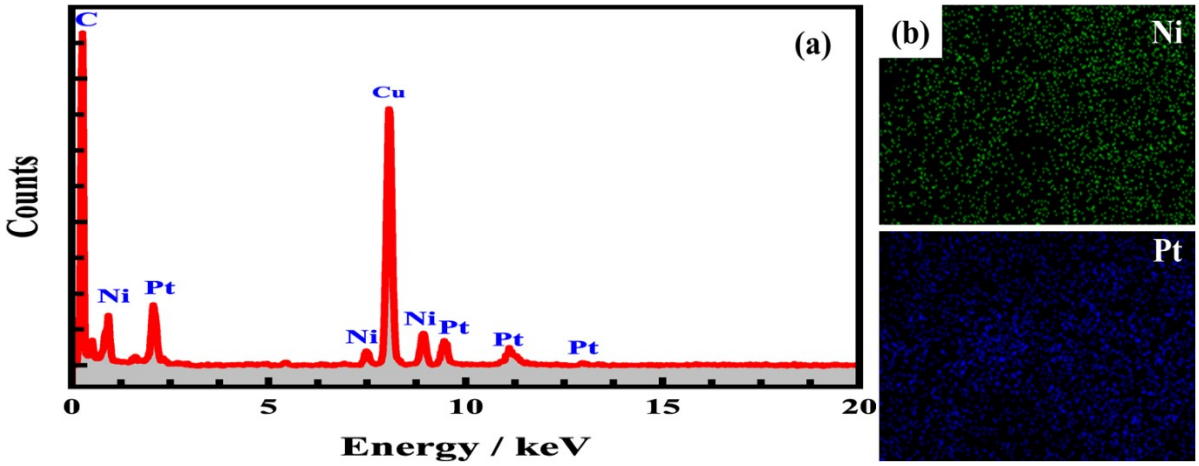

Figure S6. (a) EDX spectroscopy and (b) elemental mapping of Ni and Pt in the as-made NiPt NUCs/C catalyst after ADT.

Table S1. Summary of XRD result of NiPt NUCs/C catalyst and Pt NPs/C (E-TEK) catalyst.

Catalysts	$d_{(hkl)}$[(a)] Å			$D_{(hkl)}$[(b)] nm			$H_{(111)}/H_{(200)}$	$H_{(111)}/H_{(220)}$
	(111)	(200)	(220)	(111)	(200)	(220)		
NiPt NUCs/C	2.20	1.90	1.40	3.13	1.94	2.12	3.00	8.74
Pt NPs/C (E-TEK)	2.30	2.00	1.40	2.07	1.96	2.09	2.44	3.79

[(a)] *Calculation from Bragg's law.*

[(b)] *Calculation from Debye-Scherrer's equation.*

Table S2. Summary of fitted XPS result of as-made NiPt NUCs/C catalyst.

Catalyst	Assignment	Binding energy eV	Relative intensity %
NiPt NUCs/C	Pt^0	70.78 74.22	72.07
	Pt^{2+}	72.14 76.13	27.93
	Ni^0	853.22 870.16	35.18
	Ni^{2+}	855.88 873.55	64.82

Table S3. A comparison of ORR activity of Pt-based electrocatalysts.

Catalyst	Onset potential V_{RHE}	Half-wave potential V_{RHE}	Mass activity at 0.9 V_{RHE} mA mg_{Metal}^{-1}	Specific activity at 0.9 V_{RHE} mA cm^{-2}	Refs.
NiPt NUCs/C	0.956	0.918	565.22	1.04	This work
Pt NPs/C (E-TEK)	0.938	0.88	116.93	0.16	This work
Pd_1Pt_4 DNSs	0.99	0.89	530.0	0.74	[18]
Pt NPs/C (JM)	0.956	-	67.1	-	[19]
Pt/(Mn-N)@C	-	0.928	541.0	0.496	[20]
Pt_3Co-700	-	0.945	520.0	1.10	[21]
Pt_xY-E/C	–	0.89	483.0	0.59	[22]
La-doped Pt/C-5	–	–	490.0	0.93	[23]
D-PtNi/KB	-	0.89	460.0	1.10	[24]
Commerical Pt/C	-	0.85	180.0	0.38	[24]
Pt NPs/C	0.922	0.811	120.0	0.15	[25]
Pt-Ni NW_{Ar}/C	-	-	150.0	0.45	[26]
Pt1Co1-IMC@Pt	-	-	530.0	1.11	[27]
Pt_3Mn intermetallic/C	-	-	386.0	0.877	[28]
10% Pt/Co-N-C	-	0.886	223.0	-	[29]
$PtP_{1.4}$@Pt/C	-	0.888	310.0	0.62	[30]

Table S4. A summary of ORR performance of electrocatalysts before and after the ADT test.

Catalyst	Oxygen electro-reduction reaction				
	Half-wave potential V_{RHE}		Mass activity mA mg_{Metal}^{-1}		
	Initial	After ADT	Initial	After ADT	Deterioration %
NiPt NUCs/C	0.918	0.908	565.22	478.74	15.29
Pt NPs/C (E-TEK)	0.876	0.851	116.93	62.57	46.48

References

1. Bhuvanendran, N.; Ravichandran, S.; Zhang, W.; Ma, Q.; Xu, Q.; Khotseng, L.; Su, H., Highly efficient methanol oxidation on durable Pt_xIr/MWCNT catalysts for direct methanol fuel cell applications. *International Journal of Hydrogen Energy* **2020,** *45* (11), 6447-6460.

2. Vargas-Ordaz, M.; Velázquez-Hernández, I.; Bañuelos, J. A.; Ledesma-García, J.; Álvarez-Contreras, L.; Arjona, N.; Guerra-Balcázar, M., Synthesis of PtAg bimetallic material as a multi-fuel tolerant electrocatalyst and spectroelectrochemical analysis of its capability to perform the oxygen reduction. *Materials Today Energy* **2019,** *14*, 100335.

3. Huang, T.-H.; Bhalothia, D.; Dai, S.; Yan, C.; Wang, K.-W.; Chen, T.-Y., Bifunctional Pt–SnO_x nanorods for enhanced oxygen reduction and hydrogen evolution reactions. *Sustainable Energy & Fuels* **2021,** *5* (11), 2960-2971.

4. Bhalothia, D.; Fan, Y.-J.; Lai, Y.-C.; Yang, Y.-T.; Yang, Y.-W.; Lee, C.-H.; Chen, T.-Y., Conformational Effects of Pt-Shells on Nanostructures and Corresponding Oxygen Reduction Reaction Activity of Au-Cluster-Decorated NiO_x@Pt Nanocatalysts. *Nanomaterials* **2019,** *9* (7).

5. Zhang, C.; Zhang, Y.; Xiao, H.; Zhang, J.; Li, L.; Wang, L.; Bai, Q.; Liu, M.; Wang, Z.; Sui, N., Superior catalytic performance and CO tolerance of PtCu/graphdiyne electrocatalyst toward methanol oxidation reaction. *Colloids and Surfaces A: Physicochemical and Engineering Aspects* **2021,** *612*, 125960.

6. Huang, X.; Chen, Y.; Zhu, E.; Xu, Y.; Duan, X.; Huang, Y., Monodisperse Cu@PtCu nanocrystals and their conversion into hollow-PtCu nanostructures for methanol oxidation. *Journal of Materials Chemistry A* **2013,** *1* (46), 14449-14454.

7. Zhang, G.; Yang, Z.; Zhang, W.; Hu, H.; Wang, C.; Huang, C.; Wang, Y., Tailoring the morphology of Pt3Cu1 nanocrystals supported on graphene nanoplates for ethanol oxidation.

Nanoscale **2016,** *8* (5), 3075-3084.

8. He, Y.; Chen, W.; Li, X.; Zhang, Z.; Fu, J.; Zhao, C.; Xie, E., Freestanding Three-Dimensional Graphene/MnO_2 Composite Networks As Ultralight and Flexible Supercapacitor Electrodes. *ACS Nano* **2013,** *7* (1), 174-182.

9. Li, N.; Tang, S.; Pan, Y.; Meng, X., One-step and rapid synthesis of reduced graphene oxide supported Pt nanodendrites by a microwave-assisted simultaneous reduction. *Materials Research Bulletin* **2014,** *49*, 119-125.

10. Sahoo, L.; Mondal, S.; Gloskovskii, A.; Chutia, A.; Gautam, U. K., Unravelling charge-transfer in Pd to pyrrolic-N bond for superior electrocatalytic performance. *Journal of Materials Chemistry A* **2021,** *9* (17), 10966-10978.

11. Ometto, F. B.; Carbonio, E. A.; Teixeira-Neto, É.; Villullas, H. M., Changes induced by transition metal oxides in Pt nanoparticles unveil the effects of electronic properties on oxygen reduction activity. *Journal of Materials Chemistry A* **2019,** *7* (5), 2075-2086.

12. Ravichandran, S.; Bhuvanendran, N.; Xu, Q.; Maiyalagan, T.; Xing, L.; Su, H., Ordered mesoporous Pt-Ru-Ir nanostructures as superior bifunctional electrocatalyst for oxygen reduction/oxygen evolution reactions. *Journal of Colloid and Interface Science* **2022,** *608*, 207.

13. Da Silva, G. C.; Fernandes, M. R.; Ticianelli, E. A., Activity and Stability of Pt/IrO_2 Bifunctional Materials as Catalysts for the Oxygen Evolution/Reduction Reactions. *ACS Catalysis* **2018,** *8* (3), 2081-2092.

14. Tian, G.-L.; Zhao, M.-Q.; Yu, D.; Kong, X.-Y.; Huang, J.-Q.; Zhang, Q.; Wei, F., Nitrogen-Doped Graphene/Carbon Nanotube Hybrids: In Situ Formation on Bifunctional Catalysts and Their Superior Electrocatalytic Activity for Oxygen Evolution/Reduction Reaction. *Small* **2014,** *10* (11), 2251-2259.

15. Lu, Y.; Wen, X.; Chen, X.; Chu, P. K.; Tang, T.; Mijowska, E., Nitrogen-doped porous carbon embedded with cobalt nanoparticles for excellent oxygen reduction reaction. *Journal of Colloid and Interface Science* **2019,** *546*, 344-350.

16. Huang, Y.; Tan, Z.; Wu, H.; Feng, C.; Ding, Y., Fe@Pt core-shell nanoparticles as electrocatalyst for oxygen reduction reaction in acidic media. *Ionics* **2018,** *24* (1), 229-236.

17. Zhang, C.; Ma, B.; Zhou, Y.; Wang, C., Highly active and durable Pt/MXene nanocatalysts for ORR in both alkaline and acidic conditions. *Journal of Electroanalytical Chemistry* **2020,** *865*, 114142.

18. Peng, X.; Lu, D.; Qin, Y.; Li, M.; Guo, Y.; Guo, S., Pt-on-Pd Dendritic Nanosheets with Enhanced Bifunctional Fuel Cell Catalytic Performance. *ACS Applied Materials &*

Interfaces **2020,** *12* (27), 30336-30342.
19. Dai, S.; Chou, J.-P.; Wang, K.-W.; Hsu, Y.-Y.; Hu, A.; Pan, X.; Chen, T.-Y., Platinum-trimer decorated cobalt-palladium core-shell nanocatalyst with promising performance for oxygen reduction reaction. *Nature Communications* **2019,** *10* (1), 440.
20. Shu, Q.; Zhang, J.; Hu, B.; Deng, X.; Yuan, J.; Ran, R.; Zhou, W.; Shao, Z., Rational Design of a High-Durability Pt-Based ORR Catalyst Supported on Mn/N Codoped Carbon Sheets for PEMFCs. *Energy & Fuels* **2022,** *36* (3), 1707-1715.
21. Wang, D.; Xin, H. L.; Hovden, R.; Wang, H.; Yu, Y.; Muller, D. A.; DiSalvo, F. J.; Abruña, H. D., Structurally ordered intermetallic platinum–cobalt core–shell nanoparticles with enhanced activity and stability as oxygen reduction electrocatalysts. *Nature Materials* **2013,** *12* (1), 81-87.
22. Brandiele, R.; Guadagnini, A.; Girardi, L.; Dražić, G.; Dalconi, M. C.; Rizzi, G. A.; Amendola, V.; Durante, C., Climbing the oxygen reduction reaction volcano plot with laser ablation synthesis of PtxY nanoalloys. *Catalysis Science & Technology* **2020,** *10* (14), 4503.
23. Kim, J.; Kabiraz, M. K.; Lee, W.; Hwang, G. H.; Choi, S.-I., Solvothermal Doping of Lanthanum on Nanoscale Platinum Surfaces to Improve Oxygen Electroreduction Performance. *ChemElectroChem* **2020,** *7* (12), 2643-2650.
24. Zhao, X.; Xi, C.; Zhang, R.; Song, L.; Wang, C.; Spendelow, J. S.; Frenkel, A. I.; Yang, J.; Xin, H. L.; Sasaki, K., High-Performance Nitrogen-Doped Intermetallic PtNi Catalyst for the Oxygen Reduction Reaction. *ACS Catalysis* **2020,** *10* (18), 10637-10645.
25. Fu, S.; Zhu, C.; Song, J.; Engelhard, M. H.; Xia, H.; Du, D.; Lin, Y., Kinetically Controlled Synthesis of Pt-Based One-Dimensional Hierarchically Porous Nanostructures with Large Mesopores as Highly Efficient ORR Catalysts. *ACS Applied Materials & Interfaces* **2016,** *8* (51), 35213-35218.
26. Kato, M.; Iguchi, Y.; Li, T.; Kato, Y.; Zhuang, Y.; Higashi, K.; Uruga, T.; Saida, T.; Miyabayashi, K.; Yagi, I., Structural Transformation of Pt–Ni Nanowires as Oxygen Reduction Electrocatalysts to Branched Nanostructures during Potential Cycles. *ACS Catalysis* **2022,** *12* (1), 259-264.
27. Cheng, Q.; Yang, S.; Fu, C.; Zou, L.; Zou, Z.; Jiang, Z.; Zhang, J.; Yang, H., High-loaded sub-6 nm Pt_1Co_1 intermetallic compounds with highly efficient performance expression in PEMFCs. *Energy & Environmental Science* **2022,** *15* (1), 278-286.
28. Lim, J.; Jung, C.; Hong, D.; Bak, J.; Shin, J.; Kim, M.; Song, D.; Lee, C.; Lim, J.; Lee, H.; Lee, H. M.; Cho, E., Atomically ordered Pt3Mn intermetallic electrocatalysts for the oxygen reduction reaction in fuel cells. *Journal of Materials Chemistry A* **2022,** *10* (13),

7399.
29. Guo, P.; Liu, B.; Dai, Y.-K.; Gong, X.-F.; Xia, Y.-F.; Zhang, Y.-L.; Liu, B.; Zhao, L.; Sui, X.-L.; Wang, Z.-B., Coupling fine Pt nanoparticles and Co-Nx moiety as a synergistic bi-active site catalyst for oxygen reduction reaction in acid media. *Journal of Colloid and Interface Science* **2022,** *613*, 276-284.
30. Li, W.-Z.; Lu, B.-A.; Gan, L.; Tian, N.; Zhang, P.-Y.; Yan, W.; Chen, W.-X.; Chen, Y.-H.; Zhou, Z.-Y.; Sun, S.-G., High activity and durability of carbon-supported core-shell PtPx@Pt/C catalyst for oxygen reduction reaction. *Chinese Journal of Catalysis* **2021,** *42* (12), 2173-2180.